Free Energy Simulations of Ligand Binding to the Aspartate Transporter Glt_{Ph}

Germano Heinzelmann,[†] Turgut Baştuğ,[†‡] and Serdar Kuyucak[†*]
[†]School of Physics, University of Sydney, New South Wales, Australia; and [‡]Faculty of Arts and Sciences, TOBB University of Economy and Technology, Ankara, Turkey

ABSTRACT Glutamate/Aspartate transporters cotransport three Na^+ and one H^+ ions with the substrate and countertransport one K^+ ion. The binding sites for the substrate and two Na^+ ions have been observed in the crystal structure of the archeal homolog Glt_{Ph}, while the binding site for the third Na^+ ion has been proposed from computational studies and confirmed by experiments. Here we perform detailed free energy simulations of Glt_{Ph}, giving a comprehensive characterization of the substrate and ion binding sites, and calculating their binding free energies in various configurations. Our results show unequivocally that the substrate binds after the binding of two Na^+ ions. They also shed light into Asp/Glu selectivity of Glt_{Ph}, which is not observed in eukaryotic glutamate transporters.

INTRODUCTION

Glutamate transporters (GlTs) remove the excess extracellular glutamate using the electrochemical gradient of Na^+ ions (1). In mammalian GlTs (called excitatory amino-acid transporters, or EAATs for short), the transport mechanism involves cotransport of three Na^+ and one H^+ ions, and countertransport of one K^+ ion (2,3). A large amount of functional data has been accumulated on GlTs in the last two decades (1) but their interpretation has proved difficult in the absence of any structures. As in ion channels, the first crystal structure of a GlT was determined in prokaryotes, namely that of Glt_{Ph} from *Pyrococcus horikoshii* (4). The binding sites for the substrate and two ions were identified in a subsequent crystal structure of Glt_{Ph} (5). Initial functional studies of Glt_{Ph} revealed that the transport mechanism was independent of H^+ and K^+, but they were inconclusive on whether two or three Na^+ ions were cotransported in each cycle (5,6). This issue was settled in a recent experiment with radioactive $^{22}Na^+$ ions and [^{14}C] aspartate, which showed conclusively that three Na^+ ions are cotransported with the substrate as in EAATs (7).

Glt_{Ph} has ~36% amino-acid sequence identity with the EAATs, which is somewhat low. However, the sequence identity is much higher for the residues forming the binding pocket (~65%), and most of the residues implicated in substrate and ion binding in EAATs are conserved (8–11). Thus, in the absence of any EAAT structures, one may use the Glt_{Ph} structure to interpret the functional data from EAATs and thereby gain insights for the transport mechanism in GlTs (12,13). This can be achieved by performing detailed molecular dynamics (MD) simulations of Glt_{Ph}, where one characterizes the binding sites for the substrate and the ions and calculates their binding free energies in various configurations to determine the binding order. But before one can proceed with such a program, the binding site for the third Na^+ ion (to be called Na3) needs to be located accurately. Otherwise, a reliable prediction of the binding free energies would not be possible.

So far several MD simulations of the Glt_{Ph} structure have been carried out focusing on the opening of the extracellular gate and substrate binding (14,15), location of the Na3 site (16,17), and substrate translocation and release (18,19). The Na3 site was also searched via electrostatic calculations and valence mapping (20,21). Of the predicted Na3 sites, only those involving D312 (17,21) are completely consistent with the functional (21,22) and structural (5) data. Our initial free energy calculations indicated that even those Na3 sites did not yield binding energies that were consistent with the transport mechanism, which prompted us to further refine the Na3 site proposed in Huang and Tajkhorshid (17). The proposed new site for Na3 involves, in addition to the already identified T92, N310, and D312 side chains (17,21), two other residues, the Y89 backbone and S93 side chain. The presence of the S93 side chain in the coordination shell of the third Na^+ ion has been confirmed by S93A mutation experiments both in Glt_{Ph} and EAAT1, where a large reduction in Na^+ affinity has been observed (T. Baştuğ, G. Heinzelmann, S. Kuyucak, M. Salim, R. J. Vandenberg, and R. M. Ryan, unpublished).

It appears that all the binding sites in Glt_{Ph} have been well identified so the system is ripe for a detailed MD study. Our aim here is first to show that the MD results for the binding sites and coordination of the substrate and ions are in good agreement with the experimental data. This is important to build confidence in the model and dispel any doubts about the ion binding sites in the crystal structure where Tl^+ ions were employed instead of Na^+. We then perform free energy calculations for the substrate and ions in various configurations to determine their binding free energies,

Submitted August 30, 2011, and accepted for publication October 12, 2011.
*Correspondence: serdar@physics.usyd.edu.au
Editor: Carmen Domene.

0006-3495/11/11/2380/9 $2.00
doi: 10.1016/j.bpj.2011.10.010

which are used in predicting their binding order. In particular, a strong dependence of Asp binding to Na1 binding is found, which is explained by an H-bond network linking the two ligands. Finally, we examine the Asp/Glu selectivity in Glt_{Ph} and discuss its implications for constructing homology models for EAATs, where such an Asp/Glu selectivity is not observed.

METHODS

Model system and simulation details

Several crystal structures of the Glt_{Ph} protein are available from the Protein Data Bank. The most revealing structure is the closed structure (PDB ID: 2NWX), where an Asp and two Na^+ ions are bound and the helical hairpin 2 (HP2) gate is closed (5). Following previous MD studies (14,15), we have created an open structure from 2NWX by removing the bound Asp and Na^+ ions and observing opening of the HP2 gate in MD simulations. In a second crystal structure (PDB ID: 2NWW), the transporter inhibitor DL-threo-β-Benzyloxyaspartate is bound in place of Asp, which keeps the HP2 gate open. We have created a similar apo structure of Glt_{Ph} from 2NWW by removing the bound DL-threo-β-Benzyloxyaspartate and equilibrating the system in MD simulations. The two open structures are very similar in all respects except for the orientation of the N310 side chain, which is flipped 180° between the two structures. Because the N310 side chain is directly involved in the coordination of the Na3 site, it is important to choose the correct conformation for this side chain. The Na3 site predicted using the 2NWW structure has been shown to be more consistent with experiments (T. Baştuğ, G. Heinzelmann, S. Kuyucak, M. Salim, R. J. Vandenberg, and R. M. Ryan, unpublished). Therefore, we have adopted the conformation of the N310 side chain from the 2NWW structure in the 2NWX structure as well. With this change, the two open structures yield essentially identical results in free energy simulations.

The simulation systems are prepared using the software VMD (23). The crystal structure of the Glt_{Ph} trimer is embedded in a 1-palmitoyl-2-oleoyl-phosphatidylethanolamine phospholipid bilayer and then solvated in a box of water molecules with 125 mM of NaCl. The system contains the trimer, 239 lipid molecules, 15,688 water molecules, and 35 NaCl ions. The Glt_{Ph} trimer has a net charge of $+6e$ in the apo state. Therefore, six extra Cl^- ions are included in the apo system to maintain charge neutrality. When the bound ligands are included in simulations, neutrality of the system is preserved by adding more counterions. After the initial preparation, the system is equilibrated in two stages.

In the first stage, the coordinates of the protein atoms are fixed and the system is equilibrated with 1 atm pressure coupling in all directions until the correct water and lipid densities are obtained. At this point, the x and y dimensions of the simulation box are fixed, and pressure coupling is applied only in the z direction henceforth (typical dimensions of the simulation box are $115 \times 111 \times 71$ Å^3).

In the second stage, the protein is gradually relaxed in 2.4-ns MD simulations by reducing the restraints on the protein atoms in several steps. The system is further equilibrated for 5 ns with only a small (0.1 kcal/mol/Å^2) restraint left on the backbone atoms of the protein. This helps to preserve the structural integrity of the protein during long MD simulations. The above procedure is repeated for all structures employed in MD simulations.

MD simulation are performed using the NAMD package (Ver. 2.7b2) (24) with the CHARMM22 force field (25) including the CMAP dihedral corrections (26). The temperature is maintained at 300 K using Langevin damping with a coefficient of 5 ps^{-1}, and the pressure is kept at 1 atm using the Langevin piston method with a damping coefficient of 20 ps^{-1} (27). Periodic boundary conditions with the particle-mesh Ewald method are employed to calculate the electrostatic interactions without truncation. The Lennard-Jones (LJ) interactions are switched off between 10 and 12 Å using a smooth switching function. A time step of 2 fs is used in all MD simulations.

Free energy calculations

The standard binding free energy of a ligand can be expressed as (28–30)

$$\Delta G_{\rm b} = \Delta G_{\rm tr} + \Delta G_{\rm rot} + \Delta G_{\rm con} + \Delta G_{\rm int}, \tag{1}$$

where the first two terms represent the translational and rotational free energy differences of the ligand between the binding site and the bulk, the third term measures the free energy cost of applying conformational restraints on the ligand in the binding site relative to bulk, and the last term represents the free energy of translocating the restrained ligand from the bulk to the binding site. The translational and rotational free energy differences can be evaluated assuming Gaussian distributions for the ligand configurations in the binding site, which yields (31–34)

$$\begin{aligned} \Delta G_{tr} &= -k_{\rm B}T \ln\left[\frac{(2\pi e)^{3/2}\sigma_x\sigma_y\sigma_z}{V_0}\right], \\ \Delta G_{rot} &= -k_{\rm B}T \ln\left[\frac{(2\pi e)^{3/2}\sigma_{\phi 1}\sigma_{\phi 2}\sigma_{\phi 3}}{8\pi^2}\right], \end{aligned} \tag{2}$$

where $V_0 = 1660$ Å^3 is the reference volume for the standard concentration, σ_x, σ_y, and σ_z are the principal root mean-squared fluctuations of the center of mass of the ligand in the binding site, and $\sigma_{\phi 1}$, $\sigma_{\phi 2}$, and $\sigma_{\phi 3}$ are the rotational root mean-squared fluctuations of the ligand calculated using the quaternion representation (34). The various σ-values are estimated from MD simulations of the bound ligands without using any restraints because they are stably bound.

The free energy difference for applying conformational restraints can be written as

$$\Delta G_{\rm con} = \Delta G_{\rm con}^{\rm bulk} - \Delta G_{\rm con}^{\rm site}, \tag{3}$$

where $\Delta G_{\rm con}^{\rm bulk}$ and $\Delta G_{\rm con}^{\rm site}$ are the free energies of restraining the ligand in the bulk and the binding site, respectively. To calculate $\Delta G_{\rm con}^{\rm site}$, the equilibrium position of the ligand is determined as accurately as possible, and the heavy atoms on the ligand are restrained using $k_f = 4.5$ kcal/mol/Å^2. Following Cecchini et al. (35), these restraints are gradually relaxed and the free energy change is calculated from

$$\Delta G_{\rm con}^{\rm site} = \frac{1}{2}\int_0^{k_f} \langle |\mathbf{X} - \mathbf{X}_0|^2 \rangle dk, \tag{4}$$

where $|\mathbf{X} - \mathbf{X}_0|$ represents the difference of the restrained coordinates from the reference values at a given k. The integral is evaluated using 10 windows with $k = 4.5$, 2.0, 1.0, 0.5, 0.2, 0.1, 0.05, 0.02, 0.01, and 0 kcal/mol/Å^2. Each window is simulated for 600 ps, and the ensemble average of the coordinate difference is calculated from the last 300 ps. A similar calculation is performed in the bulk for $\Delta G_{\rm con}^{\rm bulk}$ using a box containing the ligand and 1193 water molecules (plus counterions to keep the system neutral).

The free energy of translocation, $\Delta G_{\rm int}$, is calculated using the free energy perturbation (FEP) and thermodynamic integration (TI) methods (36). In both methods, one introduces a hybrid Hamiltonian $H(\lambda) = (1 - \lambda) H_0 - \lambda H_1$, where H_0 represents the Hamiltonian for the initial (apo) state with the ligand in the bulk and H_1 for the final (ligand-bound) state. In the FEP method, the interval between $\lambda = 0$ and 1 is divided into n subintervals with $\{\lambda_i, i = 1,\ldots,n-1\}$, and for each subinterval the free energy difference is calculated from the ensemble average

$$\Delta G_i = -k_{\rm B}T \ln\left\langle \exp\left[-\frac{(H(\lambda_{i+1}) - H(\lambda_i))}{k_{\rm B}T}\right]\right\rangle_{\lambda_i}. \tag{5}$$

The free energy of translocation is obtained from the sum, $\Delta G_{\text{int}} = \sum_i \Delta G_i$. A criterion for successful application of FEP is that $\Delta G_i \lesssim 2$ kcal/mol for each window. Because charges are involved in the FEP calculations, satisfaction of this criterion would require over 130 windows if uniform subintervals are used. We have used instead exponentially spaced subintervals, which halves the required number of windows to 66. In a typical FEP calculation, each window is equilibrated for 40 ps followed by a 40-ps production run. We have used shorter and longer simulation times to check the convergence of the results in sample calculations and found that 40 + 40 ps sampling is adequate.

In the TI method, the ensemble average of the derivative, $\partial H(\lambda)/\partial\lambda$, is obtained at several λ-values, and the free energy of translocation is calculated from the integral

$$\Delta G_{\text{int}} = \int_0^1 \left\langle \frac{\partial H(\lambda)}{\partial \lambda} \right\rangle_\lambda d\lambda. \tag{6}$$

Again, because charges are involved, Gaussian quadrature provides a better method for the evaluation of this integral. In previous applications of the TI method to ion binding free energies (37), a seven-point quadrature was found to be adequate, which is also adapted here. Each window is typically equilibrated for 0.5 ns and sampled for 1 ns. Convergence of the results is checked from the running averages of the free energy differences, and the sampling runs are extended if necessary.

For Na^+ ions, application of these methods is straightforward. It is observed that the Na1 and Na3 sites in the apo structure are occupied by water molecules within a few nanoseconds of MD simulations. A similar thing happens when the Na^+ ion is removed from the Na2 site in the closed structure. This justifies alchemical transformation of a Na^+ ion in one of the binding sites to a water molecule while a water molecule in the bulk is simultaneously transformed to a Na^+ ion. To check against the hysteresis effects, we also perform the backward calculation, where a Na^+ ion in the bulk is translocated to the binding site. Thus TI calculations for each Na^+ ion took $11.5 \times 2 = 23$ ns. Convergence of the TI results is checked from the running averages (see Fig. S1 in the Supporting Material). Denoting the free energy differences obtained from the forward and backward calculations as $\Delta G_{\text{int}}^{\text{for}}$ and $\Delta G_{\text{int}}^{\text{back}}$, the free energy of translocation is obtained from their average as

$$\Delta G_{\text{int}} = \frac{1}{2}\left[-\Delta G_{\text{int}}^{\text{for}} + \Delta G_{\text{int}}^{\text{back}} \right], \tag{7}$$

and the absolute binding free energy follows upon adding the translational free energy difference

$$\Delta G_{\text{b}} = \Delta G_{\text{int}} + \Delta G_{\text{tr}}. \tag{8}$$

When Asp is removed from the open structure, the binding site is similarly flooded with water molecules in a few picoseconds. However, a direct application of the FEP method runs into convergence issues for molecules, which necessitates adoption of a staged approach to free energy calculations (30). Accordingly, Asp is restrained in the binding site and the electrostatic and LJ interactions are switched off in turn, which results in annihilation of Asp in the binding site. A reverse process is performed in the bulk simultaneously, resulting in creation of a restrained Asp in the bulk, which is then unrestrained. The reference positions for the restrained atoms are chosen so that there is a maximal overlap between the restrained and unrestrained Asp. This is demonstrated later in Table 2, where the restrained Asp (last column) is seen to have an almost identical coordination geometry as the unrestrained Asp (fifth column).

To improve convergence and prevent instabilities in the FEP calculations, we use a soft-core LJ potential with a shift coefficient of 5.0 (38). This avoids the necessity of splitting the LJ interaction into short-range and dispersion parts. We have discovered that during the backward calculation—while an uncharged Asp is created in the binding site—a water molecule gets trapped under Asp, leading to a final state inconsistent with the crystal structure. To prevent this from happening, we have inserted Asp into the binding site in two stages, first the backbone and then the side chain. A similar splitting is employed in the forward calculation—the side chain of Asp is destroyed first, followed by the backbone.

The free energy difference at each stage is calculated separately, and the forward free energy of translocation is obtained from the sum

$$\Delta G_{\text{int}}^{\text{for}} = \Delta G_{\text{elec}} + \Delta G_{\text{LJ-bb}} + \Delta G_{\text{LJ-sc}}, \tag{9}$$

where the three terms represent the contributions from the electrostatic interactions, LJ-backbone, and LJ-side chain. To calculate ΔG_{elec}, Asp in the binding site is discharged while an uncharged Asp in the bulk (30 Å away from the binding site) is charged simultaneously. We have used both FEP and TI methods for this purpose, employing the window parameters specified above. In total, four FEP and two TI simulations are performed. Evidence for convergence of the FEP results is presented in Fig. S2. In the second and third stages, the LJ interactions for the side chain and backbone of the uncharged Asp in the binding site are switched off whereas they are switched on for an uncharged Asp in the bulk. The FEP method is employed in these calculations with 52 windows for $\Delta G_{\text{LJ-sc}}$ and 44 windows for $\Delta G_{\text{LJ-bb}}$. In both cases, a shorter spacing ($\Delta\lambda = 0.01$) is used closer to the end-points to facilitate convergence. For each of the forward calculations mentioned above, a complementary backward calculation is performed to check against hysteresis. Because of the larger relative fluctuations observed, 10 independent FEP calculations are run for the LJ interactions.

We have also investigated the selectivity of Glt_{Ph} for Asp over Glu. Because all the residues that coordinate Asp in the open Glt_{Ph} are conserved in the EAATs (R276 is an exception but it coordinates with the backbone oxygen), it is assumed that Glu binds to the transporter in the same position as Asp. The free energy of mutating Asp to Glu in the binding site and bulk are determined via TI calculations as described above (except using 1-ns equilibration time for each window). The selectivity free energy is determined from the difference

$$\Delta\Delta G(\text{Asp}\rightarrow\text{Glu}) = \Delta G_{\text{Asp}\rightarrow\text{Glu}}^{\text{site}} - \Delta G_{\text{Asp}\rightarrow\text{Glu}}^{\text{bulk}}. \tag{10}$$

Note that no restraints are needed in this case, as both Asp and Glu are bound to Glt_{Ph}.

We have further simulated the Glu-bound system for 10 ns starting from the last window of the Asp → Glu transformation. Differences in the coordination of Asp and Glu in the binding pocket are examined to find out which changes are required in EAATs to accommodate Glu as well as Asp and transport it with equal efficiency.

RESULTS AND DISCUSSION

Characterization of the binding sites

We start with a comparison of the binding sites for the three Na^+ ions and Asp obtained from the MD simulations of Glt_{Ph} with those observed in the crystal structure 2NWX. The residues involved in the coordination of the Na^+ ions are listed in Table 1 together with the average Na^+–O distances obtained from 2-ns MD simulations of the closed and open structures. The main difference between the two is that the HP2 gate is open in the latter, which abolishes the Na2 site. From Table 1 it is seen that the Na3 site is tightly coordinated by one backbone and four side-chain oxygens. Note that only one of the D312 oxygens is in the first hydration shell and there are no water molecules. A similarly tight binding site is found for the Na1 site. There is a one-to-one

TABLE 1 Glt_{Ph} residues coordinating the three Na^+ ions, listed according to their binding order

Ion	Helix - Residue	Crystal structure	Closed structure	Open structure
Na3	TM3 - Y89 (O)		2.3 ± 0.1	2.3 ± 0.1
	TM3 - T92 (OH)		2.4 ± 0.1	2.4 ± 0.1
	TM3 - S93 (OH)		2.4 ± 0.1	2.3 ± 0.1
	TM7 - N310 (OD)		2.2 ± 0.1	2.2 ± 0.1
	TM7 - D312 (O_1)		2.1 ± 0.1	2.1 ± 0.1
	TM7 - D312 (O_2)		3.6 ± 0.2	3.5 ± 0.3
Na1	TM7 - G306 (O)	2.8	2.4 ± 0.2	2.4 ± 0.2
	TM7 - N310 (O)	2.7	2.3 ± 0.1	2.4 ± 0.2
	TM8 - N401 (O)	2.7	2.4 ± 0.2	2.5 ± 0.2
	TM8 - D405 (O_1)	3.0	2.2 ± 0.1	2.2 ± 0.1
	TM8 - D405 (O_2)	2.8	2.2 ± 0.1	2.3 ± 0.1
	H_2O	—	2.3 ± 0.1	2.3 ± 0.1
Na2	TM7 - T308 (O)	2.6	2.3 ± 0.1	
	TM7 - T308 (OH)	5.5	2.4 ± 0.1	
	HP2 - S349 (O)	2.1	4.5 ± 0.3	
	HP2 - I350 (O)	3.2	2.3 ± 0.1	
	HP2 - T352 (O)	2.2	2.3 ± 0.1	
	H_2O	—	2.3 ± 0.1	

Average Na^+–O distances obtained from 2-ns MD simulations of the closed and open structures are compared to those of the crystal structure (2NWX). Nature of the coordinating oxygens is indicated in parentheses; i.e., bare O denotes backbone and the others are side chain. The Na3 site is not seen in the crystal structure. The open state has Asp and two Na^+ ions bound because the Na2 site is not formed.

correspondence between the coordinating residues observed in the crystal structure and those found from the MD simulations. The larger ion-oxygen distances in the crystal structure is presumably due to the larger size of the Tl^+ ion employed in the experiments. Almost identical coordinations are obtained in the closed and open structures for the Na3 and Na1 sites, which indicates that the opening of the HP2 gate, while abolishing the Na2 site, has a minimal effect on the Na3 and Na1 sites.

Inspection of the Na2 coordination in Table 1 shows that there are some differences between the MD results and the crystal structure, which we again attribute to differences between the Tl^+ and Na^+ ions. When a Na^+ ion is placed in the experimentally observed position (to be called Na2′), it immediately shifts 2–3 Å away from the coordinating S349 backbone oxygen. With further equilibration, the side chain of T308 enters the coordination shell of Na^+, forming a very stable binding site to be called Na2 (see Fig. 1). This is observed in all three monomers, suggesting that the Na2 site is more likely to be the binding site for a Na^+ ion. The function of the Na2 site is to lock the HP2 gate in the closed conformation by binding to the residues in HP2 and TM7. In the crystal structure, this lock (the Na2′ site) has three hinges on HP2 and only one on TM7, whereas the Na2 site has two hinges on each, which provides a more reliable lock. More quantitative evidence for the proposed Na2 site will be presented below from the binding free energies.

A similar comparison is presented for the Asp binding site in Table 2. Again, there is a one-to-one correspondence

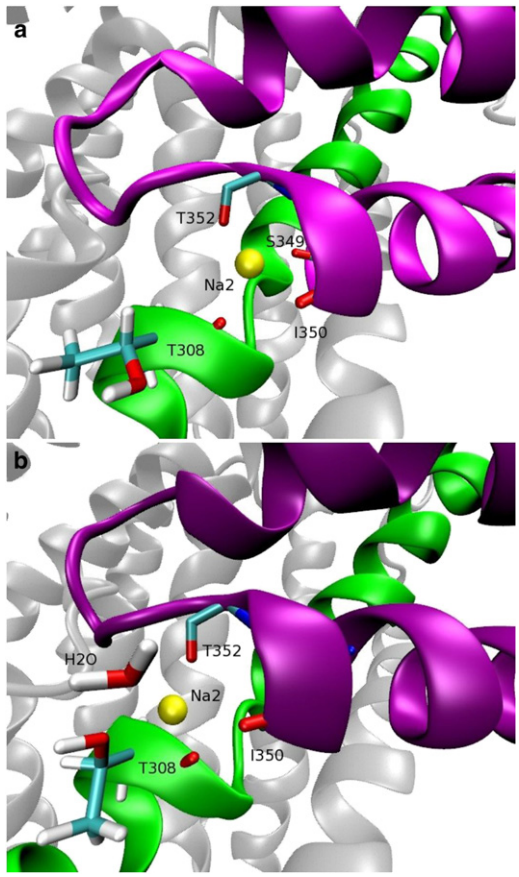

FIGURE 1 Coordination of Na2 (*a*) in the closed crystal structure of Glt_{Ph} and (*b*) in our MD simulations. See Table 1 for a list of the coordinating residues and the Na^+–O distances.

between the coordinating residues seen in the crystal structure and those found from the MD simulation of the closed state. Most of the contact distances match very well except the side chain of S278, which is found to coordinate the

TABLE 2 List of the Glt_{Ph} residues (*first column*) coordinating Asp atoms (*second column*)

Helix - Residue	Asp	Crystal structure	Closed structure	Open structure	Open structure restraints
HP1 - R276 (O)	α-N	2.4	3.0 ± 0.2	3.0 ± 0.2	3.0 ± 0.2
HP1 - S278 (N)	α-O_1	2.8	2.8 ± 0.1	2.8 ± 0.1	2.8 ± 0.1
HP1 - S278 (OH)	α-O_2	3.8	2.7 ± 0.1	2.8 ± 0.2	2.8 ± 0.1
TM7 - T314 (OH)	β-O_2	2.7	2.7 ± 0.1	2.8 ± 0.1	2.8 ± 0.1
HP2 - V355 (O)	α-N	2.9	2.9 ± 0.2	11.9 ± 0.4	11.9 ± 0.3
HP2 - G359 (N)	β-O_2	2.8	3.1 ± 0.2	6.1 ± 0.4	6.3 ± 0.3
TM8 - D394 (O_1)	α-N	2.6	2.7 ± 0.1	2.7 ± 0.1	2.7 ± 0.1
TM8 - R397 (N_1)	β-O_2	4.6	4.2 ± 0.2	2.7 ± 0.1	2.7 ± 0.1
TM8 - R397 (N_2)	β-O_1	2.5	2.9 ± 0.2	2.9 ± 0.2	2.9 ± 0.2
TM8 - T398 (OH)	α-N	3.2	3.2 ± 0.2	3.0 ± 0.2	3.0 ± 0.2
TM8 - N401 (ND)	α-O_2	2.8	2.8 ± 0.1	3.0 ± 0.2	2.9 ± 0.2

Average N–O and O–O distances obtained from the MD simulations are compared to those of the crystal structure 2NWX (*third column*). Again, bare N and O in parentheses refer to the backbone atoms and the others refer to the side-chain atoms. The last column shows the effect of the conformational restraints on the coordination of Asp.

α-carboxyl of Asp. This has been observed in other MD simulations of Glt_{Ph} as well (14,18). Below, we will show that S278 side chain plays a key role in binding of Asp following Na1. A water molecule coordinating Na1 also makes a H-bond with the S278 side chain. We speculate that absence of this water molecule in the crystal structure may have caused the shift in the position of the S278 side chain. Opening of the HP2 gate leads to the removal of the V355 and G359 residues from the coordination shell of Asp, which is partly compensated by the entry of the N_1 atom of the R397 side chain. The remaining eight contacts are preserved between the closed and open states and continue to provide a stable binding site for Asp.

Binding free energies

We first consider the binding free energies of the Na^+ ions to the sites Na1, Na2, and Na3 (Table 3). Test calculations with the FEP and TI methods have yielded essentially identical results, therefore only the TI method is used in the calculations for convenience. The forward and backward results are seen mostly to agree within 1 kcal/mol, indicating minimal hysteresis effects. The free energy difference due to loss of translational entropy remains at ~4.5–5 kcal/mol for all sites. The absolute binding free energies listed in the last column reveal that the Na3 site provides by far the largest affinity for Na^+ ions and hence it will be occupied first, followed by Na1 and Na2. It has been shown that the path to the Na3 site goes through the Na1 site (17). The 7 kcal/mol energy gradient found between the Na3 and Na1 sites here provides sufficient incentive for a Na^+ ion bound to the Na1 site to move quickly to the empty Na3 site. As shown below, the Na1 site is occupied before Asp. We have therefore calculated the binding free energy for the Na1 ion in the presence of Na3. Coulomb repulsion due to the Na3 ion results in ~4 kcal/mol increase in the binding free energy for Na1 compared to the apo state. Nevertheless this is still sufficient to provide a μM affinity for Na1.

The Na2 site is occupied last after Na3, Na1, and Asp bind, and the HP2 gate is closed. The calculated binding free energy for Na2 is higher than all the other ligands, consistent with its binding last. Because Na2 binds last, its binding free energy can be estimated from the observed enzyme rate constant, $K_m = 3.9$ mM as -3.3 kcal/mol (6), which is in good agreement with the calculated value of -2.7 kcal/mol. As argued above, the Na2 binding site found from the MD simulations is slightly different from the Na2′ site observed in the crystal structure, and the former provides a better site for binding of a Na^+ ion. Indeed the binding free energy calculated for the Na2′ site is ~5 kcal/mol higher than that of Na2, and it is positive. This provides quantitative evidence that the Na2 site is more likely to be the actual binding site. We note that the T308 side chain—proposed to be involved in coordination of the Na2 site here—is highly conserved in the EAATs and may not have been resolved in the crystal structure due to the replacement of Na^+ by the larger Tl^+ ion. This hypothesis could be confirmed in future experiments by mutating T308 to a nonpolar residue and observing how the Na^+ affinity and the Asp transport rate are affected by this mutation.

The results of the binding free energy calculations for Asp are presented in Table 4. As discussed below, Asp binds only in the presence of Na1 and Na3, therefore the calculations are performed only for this configuration. To ensure the reliability of the electrostatic calculations, we have determined it using both the FEP and TI methods. As seen from Table 4, the two methods yield consistent results. Electrostatic interactions dominate the binding of Asp resulting in a tightly bound ligand. This happens at the expense of the LJ interactions, which, therefore make a positive contribution (4.6 kcal/mol) to the binding energy. The translational and rotational free energy losses are even more significant, reducing the binding free energy by a further 7.2 kcal/mol. Comparable results have been obtained for the entropic free energy losses for similar-sized ligands (30). Finally, the conformational restraints make a relatively small contribution to the binding free energy, reflecting the fact that Asp is slightly more restrained in the binding site compared to the bulk. We note that the measured binding free energy of Asp, –12 kcal/mol (5), refers to the closed state of Glt_{Ph}, which includes the free energies of gate-closure and Na2 binding. The calculated free energy is for the binding of Asp to the open state of Glt_{Ph}. Therefore, a direct comparison with experiment is not possible at this stage. Binding free energy calculations that include the gating free energy have been performed for a glutamate receptor recently (39). We are planning similar calculations for the HP2 gate in Glt_{Ph}, which will enable comparison with experiments.

TABLE 3 Binding free energies for Na^+ ions in the open state (for Na3 and Na1) and closed state (for Na2) of Glt_{Ph} (in kcal/mol)

Ion	$-\Delta G^{for}_{int}$	ΔG^{back}_{int}	ΔG_{int}	ΔG_{tr}	ΔG_b
Na3	−22.3 ± 1.2	−24.2 ± 0.9	−23.3 ± 1.1	4.6	−18.7 ± 1.1
Na1	−15.9 ± 0.9	−16.5 ± 1.6	−16.2 ± 1.3	4.9	−11.3 ± 1.3
Na1 (3)	−11.8 ± 1.6	−11.9 ± 0.9	−11.9 ± 1.3	4.8	−7.1 ± 1.3
Na2 (1, 3, Asp)	−6.6 ± 1.3	−7.7 ± 1.3	−7.1 ± 1.3	4.4	−2.7 ± 1.3
Na2′ (1, 3, Asp)	−1.4 ± 0.9	−2.1 ± 0.8	−1.7 ± 0.8	4.4	+2.7 ± 0.8

Various contributions to the binding free energy as described in Eqs. 7 and 8 are listed separately. Other ligands present in the transporter are indicated in parentheses. Errors are estimated from block data analysis using 100-ps windows.

TABLE 4 Binding free energy of aspartate in the open state of Glt_{Ph} with the Na1 and Na3 sites occupied (in kcal/mol)

ΔG_{elec} (FEP)	ΔG_{elec} (TI)	$\Delta G_{LI\text{-}bb}$	$\Delta G_{LI\text{-}sc}$	ΔG_{tr}	ΔG_{rot}	ΔG_{con}	ΔG_{b}
−15.8 ± 0.6	−16.4 ± 0.9	3.8 ± 0.5	0.8 ± 0.5	3.3	3.9	0.5	−3.8 ± 1.0

Forward and backward calculations differed <1 kcal/mol in all cases, therefore only their average is listed. The electrostatic contribution is taken as the average of the FEP and TI results given in the first two columns. The absolute binding free energy of Asp is given in the last column.

Role of Na1 in facilitating Asp binding

We have also attempted to calculate the binding free energy of Asp in the presence of Na3 only, but failed to stabilize Asp in the binding site in the absence of Na1. Na1 is not directly involved in the coordination of Asp, so the cause of this instability is not immediately clear. A careful study of this phenomenon has revealed a close relationship between the binding of Asp and the occupation of the Na1 site, namely, a network of hydrogen bonds that pin down Asp in the binding site is only stable in the presence of Na1. This H-bond network is indicated by a dashed line in Fig. 2, which shows the binding site of Asp obtained from the equilibrium simulations of the open structure with Asp, Na1, and Na3 bound. It is seen from Fig. 2 that the water molecule that coordinates the Na1 ion also makes a H-bond with the side-chain oxygen of S278, which, in turn, initiates the following chain of H-bonds: S278 (HG)-Asp (α-O_2)-N401 (HD_2); N401 (HD_1)-T314 (OG); and T314 (HG)-Asp (β-O_2)-R397 (HN). The net effect of the H-bond network is to firmly anchor the backbone and side-chain oxygens of Asp to the protein via four H-bonds. This network of H-bonds remains very stable throughout the simulations of the open structure, as indicated by the average O–H distances (see Table S1 in the Supporting Material).

To see how removal of the Na1 ion destabilizes and unzips the H-bond network, we have performed MD simulations of the system after removing the Na1 ion with only Na3 and Asp present. Initially 4 kcal/mol/Å^2 restraints are applied to all the C and N atoms of Asp, which are gradually relaxed during 2 ns of MD simulations. The system is then run for a further 3 ns with no restraints applied, during which time Asp is observed to unbind in all three monomers. The sequence of events leading to the collapse of the H-bond network and release of Asp are as follows (see Fig. S3 for the snapshots):

1. After 1 ns of simulations when the restraints on Asp are 1 kcal/mol/Å^2 (see Fig. S3 *a*): a water molecule is near the Na1 site now with its hydrogens facing the Na1 site and its oxygen directed toward the S278 side chain. This causes the S278 side chain to break the H-bond with Asp (α-O_2) and make an H-bond with the water oxygen instead.
2. At 2 ns with no restraints (see Fig. S3 *b*): Sideway motion of S278 allows entry of a water molecule to the binding site. This water molecule breaks the Asp (α-O_2)-N401 (HD_2) H-bond, and starts making H-bonds with these two atoms and S278 (OG). Freeing of the N401 side chain disrupts the N401 (HD_1)-T314 (OG) H-bond, which, in turn, destabilizes the T314 side chain. Entry of another water molecule (not shown) helps to break the T314 (HG)-Asp (β-O_2) H-bond, with T314 side chain now making a H-bond with this water molecule. At this stage, α-O_2 of Asp is free, and mobility of Asp has increased considerably.
3. At 2.5 ns (see Fig. S3 *c*): The two contacts from the β-carboxyl group of Asp to the R397 side chain are lost, leaving it completely free. Only four out of the nine contacts are still intact, namely, S278 (N) that coordinates α-O_1, and R276 (O), D394 (O_1) and T398 (OH) that coordinate α-N. More water molecules enter the binding site, further destabilizing Asp.
4. At 3.6 ns (see Fig. S3 *d*): The remaining contacts are also lost. The binding site is now full of water molecules, and Asp is released to the solvent.

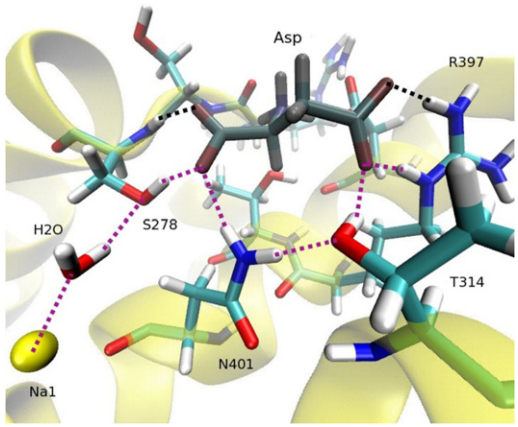

FIGURE 2 Binding site of Glt_{Ph} in the open state, with aspartate (*dark-shaded*) bound. (*Dotted lines*) Hydrogen bonds. (*Light-shade bonds*) Chain of H-bonds that stabilizes Asp in the binding site in the presence of Na1. The three contacts to the substrate α-amino group are not shown. This structure is stable throughout the simulations performed in the open state, as shown in Table S1 in the Supporting Material.

The above mechanism could play a role in the binding/unbinding of Asp. To appreciate its potential significance, we note that none of the Na^+ ions in Glt_{Ph} is in direct contact with Asp, which makes it difficult to understand the physical basis of the Asp–Na^+ coupling in glutamate transporters. For example, in LeuT transporters, a Na^+ ion is in direct contact with the substrate, which makes their coupling obvious (40). Here the Na1 ion is separated from Asp by a water molecule and a hydroxyl side chain but they are

nevertheless coupled through the H-bond network depicted in Fig. 2. Removal of the Na1 ion triggers the unzipping of the H-bond network and simultaneous entry of water molecules to the binding site, which facilitate the unbinding of Asp. A likely scenario for binding of Asp is to follow this script in reverse, that is, Asp binds to Glt_{Ph} after Na1, following the steps 1–4 in the reverse direction. Experimental evidence for the key role played by the S278 side chain in the binding of Asp comes from cysteine scanning experiments in EAAT2 (41). Mutation of the residue corresponding to S278 in EAAT2 (S363) to cysteine results in 100-fold reduction in the transport activity.

In a recent crystal structure of Glt_{Ph}, the transporter was captured in the inward-facing conformation. This structure has indicated that HP1 is most likely to be the intracellular gate, functioning in a similar fashion to the extracellular HP2 gate (42). A similar conclusion has also been reached from modeling studies (19,43). Inspection of Table 2 shows that three residues in HP1 coordinate Asp, including the S278 side chain that plays a key role in the H-bond network. Thus opening of HP1 will not only remove these three contacts from Asp but will also lead to the unzipping of the H-bond network, further destabilizing Asp. In the light of the above discussions, we suggest that Asp should unbind quite fast and may even be the first ligand to vacate the binding pocket.

Aspartate/Glutamate selectivity

The bacterial transporter Glt_{Ph} does not transport Glu, which is the main substrate for the mammalian GlTs (EAATs). To build a homology model of EAATs based on Glt_{Ph}, one needs to understand why Glu is not transported by Glt_{Ph}, and find the differences in structures that enable EAATs to transport both substrates. Fig. 3 shows the results obtained from 10-ns MD simulations with Glu bound to the open and closed states of Glt_{Ph}. In the open state, the three contacts that coordinate the Asp side chain, two from R397 and one from T314, do not coordinate Glu, even though Glu stays bound to the transporter. The longer side chain of Glu does not quite fit in the binding pocket, resulting in the loss of these contacts. Mutagenesis experiments on the R447 residue in EAAT3 (equivalent to R397 in Glt_{Ph}) have shown that interaction of this residue with the side-chain carboxyl of Glu is of critical importance for transport (10), which is prevented in the open state of Glt_{Ph} due to space constraints. Closing of the HP2 gate (Fig. 3 *b*) induces a conformational change in the Glu side chain such that the contacts with the R397 and T314 side chains are restored.

When this conformation of Glu is placed in the open state and equilibrated, it goes back to the original open-state conformation (Fig. 3 *a*) within a few picoseconds of releasing the restraints. This indicates that Glu is in a higher energy conformation in the closed state. However, even in this conformation, the Glu side chain does not fit in the binding

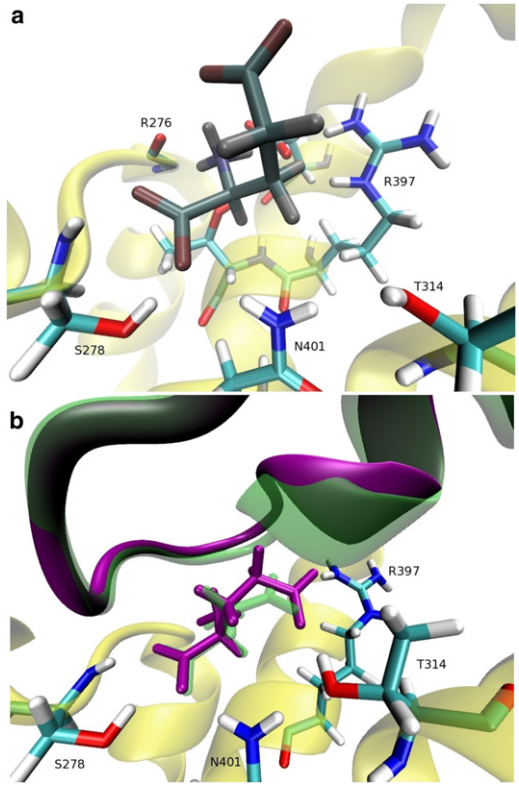

FIGURE 3 Binding site of Glt_{Ph} with a bound Glu in the open and closed states. (*a*) Open state: Residues R397 and T314, which coordinate the β-carboxyl group of Asp, do not coordinate Glu (*dark shaded*), resulting in a lower binding affinity for Glu. (*b*) Closed state: The side chain of Glu (*dark shaded*) sticks out further relative to Asp (*transparent light shaded*), resulting in displacement of the HP2 residues (*dark shaded*) with respect to the Asp-bound case (*transparent light shaded*).

pocket as well as Asp, resulting in displacement of the HP2 gate by ~1.5 Å relative to the Asp-bound case (Fig. 3 *b*). These observations suggest that the binding pocket in EAATs must be larger or more flexible to accommodate Glu. Sequence alignment indicates that majority of the residues forming the binding pocket are conserved, and the only residue that may have an effect on the volume is R276 in GltPh, which is replaced by A or S in EAATs. The R276 side chain is located between HP1 and TM8 and its replacement by a smaller side chain may help to increase the volume of the binding pocket.

For a quantitative assessment of the perturbations caused by the binding of Glu, we have calculated the free-energy required to mutate Asp to Glu in the open and closed structures of Glt_{Ph} (listed in Table 5). In the open state, the binding free energy difference between Asp and Glu is $\Delta G^{op}_{Asp\rightarrow Glu} = 5.2$ kcal/mol. Using the binding free energy of Asp (−3.8 kcal/mol), we can estimate the binding free energy of Glu as +1.4 kcal/mol. However, for the reasons stated above for Asp, this result cannot be directly compared to the experimental value for Glu binding. In the closed state, the binding free energy difference is given by

TABLE 5 Asp → Glu selectivity in the binding site for the open state of Glt_{Ph} with Na1 and Na3 bound, and the closed state with all the ions bound to the transporter

Glt_{Ph} state	ΔG^{for}_{int}	$-\Delta G^{back}_{int}$	ΔG^{av}_{int}	ΔG_{tr}	ΔG_{rot}	$\Delta G_{Asp\rightarrow Glu}$
Open	5.3 ± 1.1	5.3 ± 1.6	5.3 ± 1.3	0.0	−0.1	5.2 ± 1.3
Closed	6.3 ± 1.4	5.7 ± 1.7	6.0 ± 1.5	−0.1	−0.5	5.4 ± 1.5

Second column gives the free energy of mutating Asp to Glu in the binding site, minus the free energy of doing the same in the bulk. The third column gives the same for the backward transition. The average of the two is listed in the fourth column. The next two columns give the translational and rotational free energy differences between Asp and Glu, and the last column gives the total selectivity free energy. Errors are estimated from block data analysis using 100-ps windows.

$\Delta G^{cl}_{Asp\rightarrow Glu} = 5.4$ kcal/mol. The experimental value obtained from the ratio of the dissociation constants of Asp and Glu is 6.6 kcal/mol (5), which is close to the calculated binding free energy difference.

Because we know the free-energy of mutating Asp to Glu in the closed and open states, we can estimate the difference in free energy of gating between the Asp and Glu-bound configurations. Using the thermodynamic cycle, this quantity can be written as

$$\Delta G^{op\rightarrow cl}_{Glu} - \Delta G^{op\rightarrow cl}_{Asp} = \Delta G^{cl}_{Asp\rightarrow Glu} - \Delta G^{op}_{Asp\rightarrow Glu}. \quad (11)$$

From the values given in Table 5, it is seen that the gating energy remains about the same when Glu is bound compared to the Asp-bound case. It will be interesting to calculate the individual gating energies for the Asp-bound and Glu-bound cases from umbrella-sampling MD simulations (39) and compare the substrate-binding free energies directly to the experimental results.

CONCLUSIONS

We have performed free energy simulations for the Asp transporter Glt_{Ph}, a homolog of the mammalian glutamate transporters (EAATs). We have investigated in detail the coordination of all the ligands and calculated their binding free energies. The coordination shells found for Asp and Na1 in the closed state are in good agreement with the crystal structure. A small displacement of the experimental Na2 site is observed, which results in replacement of the S349 carbonyl in the coordination shell with the T308 hydroxyl. The new Na2 site is shown to be more stable and also more consistent with the gate-locking function of Na2.

Our simulations show that Asp is firmly bound to the open structure in the presence of Na3 and Na1 but becomes unstable when Na1 is removed, unbinding in <5 ns in all three monomers. A close scrutiny of the unbinding process has revealed that Na1 and Asp are coupled via a hydrogen-bond network, and removal of Na1 leads to the unzipping of this network destabilizing Asp. The binding sequence of the ligands is determined from their binding free energies as: Na3, Na1, Asp (HP2 gate closes), and Na2. The binding order of the second Na^+ ion and Asp has not been resolved from experimental observations and previous MD simulations (17). Our results clearly show that Asp binding is contingent upon the presence of Na1, and this happens after the binding of the second Na^+ ion. Finally, our MD simulations with bound Glu and FEP calculations for transforming Asp→ Glu in the open and closed states provide a simple mechanistic explanation for why Glt_{Ph} transports Asp but not Glu—the binding pocket is too small to accommodate the larger Glu, which remains in a higher energy state compared to Asp both in the open and closed states. The insights provided for Asp/Glu selectivity here will provide valuable guidance in constructing homology models for EAATs based on the Glt_{Ph} structure.

SUPPORTING MATERIAL

One table and three figures are available at http://www.biophysj.org/biophysj/supplemental/S0006-3495(11)01199-4.

Calculations were performed using the High-Performance Computing facilities at the National Computational Infrastructure (Canberra) and ULAKBIM (Ankara). We thank Rob Vandenberg and Renae Ryan for discussions on the structure and function of Glt_{Ph}.

This work was supported by grants from the Australian Research Council and Turkish Scientific and Technical Research Council.

REFERENCES

1. Danbolt, N. C. 2001. Glutamate uptake. *Prog. Neurobiol.* 65:1–105.
2. Kanner, B. I., and A. Bendahan. 1982. Binding order of substrates to the sodium and potassium ion coupled L-glutamic acid transporter from rat brain. *Biochemistry.* 21:6327–6330.
3. Zerangue, N., and M. P. Kavanaugh. 1996. Flux coupling in a neuronal glutamate transporter. *Nature.* 383:634–637.
4. Yernool, D., O. Boudker, …, E. Gouaux. 2004. Structure of a glutamate transporter homologue from *Pyrococcus horikoshii*. *Nature.* 431: 811–818.
5. Boudker, O., R. M. Ryan, …, E. Gouaux. 2007. Coupling substrate and ion binding to extracellular gate of a sodium-dependent aspartate transporter. *Nature.* 445:387–393.
6. Ryan, R. M., E. L. Compton, and J. A. Mindell. 2009. Functional characterization of a Na^+-dependent aspartate transporter from *Pyrococcus horikoshii*. *J. Biol. Chem.* 284:17540–17548.
7. Groeneveld, M., and D. J. Slotboom. 2010. Na^+: aspartate coupling stoichiometry in the glutamate transporter homologue Glt_{Ph}. *Biochemistry.* 49:3511–3513.
8. Vandenberg, R. J., J. L. Arriza, …, M. P. Kavanaugh. 1995. Constitutive ion fluxes and substrate binding domains of human glutamate transporters. *J. Biol. Chem.* 270:17668–17671.
9. Kavanaugh, M. P., A. Bendahan, …, B. I. Kanner. 1997. Mutation of an amino acid residue influencing potassium coupling in the glutamate transporter GLT-1 induces obligate exchange. *J. Biol. Chem.* 272:1703–1708.
10. Bendahan, A., A. Armon, …, B. I. Kanner. 2000. Arginine 447 plays a pivotal role in substrate interactions in a neuronal glutamate transporter. *J. Biol. Chem.* 275:37436–37442.

11. Seal, R. P., B. H. Leighton, and S. G. Amara. 2000. A model for the topology of excitatory amino acid transporters determined by the extracellular accessibility of substituted cysteines. *Neuron.* 25:695–706.
12. Forrest, L. R., R. Krämer, and C. Ziegler. 2011. The structural basis of secondary active transport mechanisms. *Biochim. Biophys. Acta.* 1807:167–188.
13. Jiang, J., and S. G. Amara. 2011. New views of glutamate transporter structure and function: advances and challenges. *Neuropharmacology.* 60:172–181.
14. Shrivastava, I. H., J. Jiang, …, I. Bahar. 2008. Time-resolved mechanism of extracellular gate opening and substrate binding in a glutamate transporter. *J. Biol. Chem.* 283:28680–28690.
15. Huang, Z., and E. Tajkhorshid. 2008. Dynamics of the extracellular gate and ion-substrate coupling in the glutamate transporter. *Biophys. J.* 95:2292–2300.
16. Larsson, H. P., X. Y. Wang, …, S. Y. Noskov. 2010. Evidence for a third sodium-binding site in glutamate transporters suggests an ion/substrate coupling model. *Proc. Natl. Acad. Sci. USA.* 107:13912–13917.
17. Huang, Z., and E. Tajkhorshid. 2010. Identification of the third Na^+ site and the sequence of extracellular binding events in the glutamate transporter. *Biophys. J.* 99:1416–1425.
18. Gu, Y., I. H. Shrivastava, …, I. Bahar. 2009. Molecular simulations elucidate the substrate translocation pathway in a glutamate transporter. *Proc. Natl. Acad. Sci. USA.* 106:2589–2594.
19. DeChancie, J., I. H. Shrivastava, and I. Bahar. 2011. The mechanism of substrate release by the aspartate transporter Glt_{Ph}: insights from simulations. *Mol. Biosyst.* 7:832–842.
20. Holley, D. C., and M. P. Kavanaugh. 2009. Interactions of alkali cations with glutamate transporters. *Philos. Trans. R. Soc. Lond. B Biol. Sci.* 364:155–161.
21. Tao, Z., N. Rosental, …, C. Grewer. 2010. Mechanism of cation binding to the glutamate transporter EAAC1 probed with mutation of the conserved amino acid residue Thr^{101}. *J. Biol. Chem.* 285:17725–17733.
22. Tao, Z., Z. Zhang, and C. Grewer. 2006. Neutralization of the aspartic acid residue Asp-367, but not Asp-454, inhibits binding of Na^+ to the glutamate-free form and cycling of the glutamate transporter EAAC1. *J. Biol. Chem.* 281:10263–10272.
23. Humphrey, W., A. Dalke, and K. Schulten. 1996. VMD: visual molecular dynamics. *J. Mol. Graph.* 14:33–38, 27–28.
24. Phillips, J. C., R. Braun, …, K. Schulten. 2005. Scalable molecular dynamics with NAMD. *J. Comput. Chem.* 26:1781–1802.
25. MacKerell, Jr., A. D., D. Bashford, …, M. Karplus. 1998. All-atom empirical potential for molecular modeling and dynamics studies of proteins. *J. Phys. Chem. B.* 102:3586–3616.
26. Mackerell, Jr., A. D., M. Feig, and C. L. Brooks, 3rd. 2004. Extending the treatment of backbone energetics in protein force fields: limitations of gas-phase quantum mechanics in reproducing protein conformational distributions in molecular dynamics simulations. *J. Comput. Chem.* 25:1400–1415.
27. Feller, S., Y. Zhang, …, B. Brooks. 1995. Constant pressure molecular dynamics: the Langevin piston method. *J. Chem. Phys.* 103:4613–4621.
28. Gilson, M. K., J. A. Given, …, J. A. McCammon. 1997. The statistical-thermodynamic basis for computation of binding affinities: a critical review. *Biophys. J.* 72:1047–1069.
29. Boresch, S., F. Tettinger, …, M. Karplus. 2003. Absolute binding free energies: a quantitative approach for their calculation. *J. Phys. Chem. B.* 107:9535–9551.
30. Deng, Y., and B. Roux. 2006. Calculation of standard binding free energies: aromatic molecules in T4 lysozyme L99A mutant. *J. Chem. Theory Comput.* 2:1255–1273.
31. Karplus, M., and J. N. Kushick. 1981. Methods for estimating the configurational entropy of macromolecules. *Macromolecules.* 14:325–332.
32. Luo, H., and K. Sharp. 2002. On the calculation of absolute macromolecular binding free energies. *Proc. Natl. Acad. Sci. USA.* 99:10399–10404.
33. Carlsson, J., and J. Aqvist. 2005. Absolute and relative entropies from computer simulation with applications to ligand binding. *J. Phys. Chem. B.* 109:6448–6456.
34. Minh, D. D. L., J. M. Bui, …, J. A. McCammon. 2005. The entropic cost of protein-protein association: a case study on acetylcholinesterase binding to fasciculin-2. *Biophys. J.* 89:L25–L27.
35. Cecchini, M., S. V. Krivov, …, M. Karplus. 2009. Calculation of free-energy differences by confinement simulations. Application to peptide conformers. *J. Phys. Chem. B.* 113:9728–9740.
36. Beveridge, D. L., and F. M. DiCapua. 1989. Free energy via molecular simulation: applications to chemical and biomolecular systems. *Annu. Rev. Biophys. Biophys. Chem.* 18:431–492.
37. Baştuğ, T., and S. Kuyucak. 2006. Energetics of ion permeation, rejection, binding, and block in gramicidin A from free energy simulations. *Biophys. J.* 90:3941–3950.
38. Zacharias, M., T. P. Straatsma, and J. A. McCammon. 1994. Separation-shifted scaling, a new scaling method for Lennard-Jones interactions in thermodynamic integration. *J. Chem. Phys.* 100:9025–9031.
39. Lau, A. Y., and B. Roux. 2011. The hidden energetics of ligand binding and activation in a glutamate receptor. *Nat. Struct. Mol. Biol.* 18: 283–287.
40. Yamashita, A., S. K. Singh, …, E. Gouaux. 2005. Crystal structure of a bacterial homologue of Na^+/Cl^- dependent neurotransmitter transporters. *Nature.* 437:215–223.
41. Grunewald, M., and B. I. Kanner. 2000. The accessibility of a novel reentrant loop of the glutamate transporter GLT-1 is restricted by its substrate. *J. Biol. Chem.* 275:9684–9689.
42. Reyes, N., C. Ginter, and O. Boudker. 2009. Transport mechanism of a bacterial homologue of glutamate transporters. *Nature.* 462:880–885.
43. Crisman, T. J., S. Qu, …, L. R. Forrest. 2009. Inward-facing conformation of glutamate transporters as revealed by their inverted-topology structural repeats. *Proc. Natl. Acad. Sci. USA.* 106:20752–20757.